International Journal of Environmental Sciences
ISSN: 2229-7359
Vol. 11 No. 17s, 2025
https://theaspd.com/index.php

Numerical Investigation Of Permeability Effects On Blood Flow In A Stenosed Artery Using The Crank-Nicolson Method

Anil Kumar[1], Akash[2], Ram Bharat Singh[3], Anshu Murarka[4]
[1, 3]Department of Applied Sciences and Humanities, IMS Engineering College, Ghaziabad- 201009, UP, India, dranilkumar73@rediffmail.com[1], rambharat.maths@gmail.com[3]
[2]Department of Mathematics, Starex University Gurugram-122413, Haryana, India, singh475@gmail.com
[4]Department of Applied Sciences and Humanities, Pillai College of Engineering, New Panvel , Navi Mumbai , Maharashtra India, smurarkal@rediffmail.com

Abstract:
The flow dynamics in a stenosis artery with an obstruction are solved using a finite difference technique in this study, taking the permeability parameter's effects into account. The Crank-Nicolson method is used to solve the governing equations. With special attention to the impact of porosity, the results are interpreted in the context of blood flow through a stenosis artery. High shear stress is unlikely to cause atherosclerotic lesions, according to quantitative numerical models for both steady and pulsatile flows. The role of porosity is found to be significant, especially in conditions related to cholesterol accumulation and related arterial diseases.
Key words: *Crank- Nicholson technique, cholesterol, porosity, stenosed artery, Gauss-Siedal method.*

1. INTRODUCTION

The pressure and flow conditions affect the structure, mechanical characteristics, and geometry of the artery wall and blood vessels. General stenosis arteries remodel their functional properties in response to prolonged changes in flow pressure. Because atherosclerotic vessels pose a serious risk to health and are a leading cause of death and morbidity in the developed world, the homodynamics of flow through these channels is of great interest. It is impossible to overlook the impact of porosity on blood flow when examining a real-world issue. The artery narrowing that occurs locally is a hallmark of atherosclerotic disease. The development of lesions in affected arteries causes deposits to build up on the arterial walls. It becomes crucial to effectively control and analyze flow behavior as the blood flow channel gets restricted. Understanding arterial flow has been aided by a number of important research, which are outlined below: Bharadvaj et al. (1982a, b) utilized flow visualization techniques and Laser Doppler velocity measurements to investigate arterial flow characteristics. Rindt et al. (1987) conducted both experimental and numerical studies on two-dimensional steady and pulsatile flow in a similar configuration. Rieu et al. (1989) demonstrated that bifurcating flow in a rectangular channel model closely resembles flow bifurcation in circular cylinders. Reuderink (1991) presented computational results for pulsatile flow in a three-dimensional, distensible model of the carotid artery bifurcation. Boesiger et al. (1992) employed magnetic resonance imaging (MRI) to study arterial hemodynamics. Banerjee et al. (1993) investigated blood flow in the femoral artery. Perktold and Rappitsch (1995) successfully applied numerical methods to study arterial flow phenomena, incorporating complex factors such as non-Newtonian behavior and vessel wall distensibility. Sharma and Kapur (1995) conducted a mathematical analysis of blood flow through arteries using the Finite Element Method. Botnar et al. (1996) addressed geometric image artifacts and showed that using a partial echo acquisition scheme with shortened echo time reduces flow quantification errors under complex flow conditions. The flow of blood through stenosed arteries has been a topic of significant research interest due to the elevated fluid shear stresses occurring near the stenosis neck or throat,

which can activate platelets and induce thrombosis (Ku, 1997). Rachev et al. (1998) proposed a model addressing the geometric and mechanical adaptation of arteries, while Reese and Thompson (1998) applied a simplified model based on laminar boundary layer theory to examine blood flow through arterial stenoses at Reynolds numbers up to 1000. Zendehbudi and Moayery (1999) compared physiological and simplified pulsatile flows through stenosed arteries. Botnar et al. (2000) investigated the role of different flow patterns in the initiation and progression of atherosclerotic plaque deposition by correlating MRI velocity measurements with numerical simulations. Advancements in both numerical techniques and experimental tools—such as the Laser Doppler Anemometer (LDA)—have significantly improved the measurement and analysis of arterial flows. Huang et al. (1995) utilized an LDA to measure velocity and employed pressure transducer tape to measure wall pressure at selected locations along a Plexiglas model of a constricted tube. A finite difference technique is employed, incorporating a boundary-fitted coordinate transformation to map the irregular geometry from the physical domain to a unit square in the computational domain. The vorticity–stream function formulation of the governing equations is solved numerically. Following the methodology of Sharma and Kapur (1995), the transformed equations and boundary conditions subject to a transverse magnetic field are solved using the standard finite difference scheme. A performance and analysis of carotid artery blood flow and its application were conducted by Gupta (2011). Finite element Galerkin's technique for flow in blood arteries with magnetic effects was examined by Gupta (2009). Anil Kumar and R. K. Saket (2008) looked at the convective diffusion mechanism' dependability in porous blood arteries. A computational method for flow in blood arteries with porous effects was proposed by Kumar et al. (2005). Blood flow in elastic arteries was analyzed and performance modeled by Kumar et al. (2005). Salahuddin et al. (2025) used a porous medium with heat generation to analyze blood flow in stenotic arteries. Lubna Sarwar, Sarwar and Azad (2023) founded flow physical appearance of Au-blood nanofluid in stenotic artery.

In the present study, the fluid dynamics of a stenosed artery are simulated by analyzing incompressible flow through an axisymmetric, rigid tube with a smooth constriction, under the influence of a transverse magnetic field. The analysis considers physiological ranges of Reynolds number and frequency parameters.

2.1 Governing Equations

The non-dimensional form of the governing Navier–Stokes momentum equations, along with the continuity equation, is expressed in cylindrical coordinates as follows:

$$\frac{2\alpha^2}{\mathrm{Re}}\frac{\partial u}{\partial t}+u\frac{\partial u}{\partial x}+v\frac{\partial u}{\partial y}=-\frac{\partial p}{\partial x}+\frac{2}{\mathrm{Re}}\left(\frac{\partial\, u}{\partial x}+\frac{\partial\, u}{\partial y}+\frac{1}{y}\frac{\partial u}{\partial y}\right)-\mathrm{K}u \tag{1}$$

$$\frac{2\alpha^2}{\mathrm{Re}}\frac{\partial v}{\partial t}+u\frac{\partial v}{\partial x}+v\frac{\partial v}{\partial y}=-\frac{\partial p}{\partial y}+\frac{2}{\mathrm{Re}}\left(\frac{\partial^2 v}{\partial x^2}+\frac{\partial^2 v}{\partial y^2}+\frac{1}{y}\frac{\partial v}{\partial y}-\frac{v}{y^2}\right)-\mathrm{K}v \tag{2}$$

$$\frac{\partial u}{\partial x}+\frac{\partial v}{\partial y}=\frac{v}{y}, \tag{3}$$

where u and v are the axial and radial velocity components, p is the pressure, and K is the permeability parameter . The Reynolds number and Womersley number are defined as,

$\mathrm{Re}=\frac{2U}{\nu}$, $\alpha=R\left(\frac{\omega}{\nu}\right)^{\frac{1}{2}}$ respectively, where U average velocity, R radius of the artery in an upstream location of the stenosis and ν kinematic viscosity of the blood.

International Journal of Environmental Sciences
ISSN: 2229-7359
Vol. 11 No. 17s, 2025
https://theaspd.com/index.php

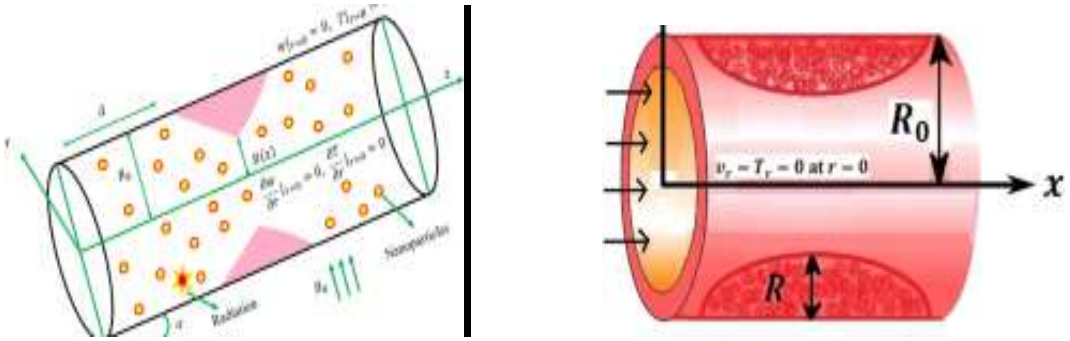

(a) (b)

Figure 1. Geometrical structure of Stenosis artery

The stream function–vorticity formulation of the Navier–Stokes equations offers a significant advantage over the primitive variable form in solving two-dimensional incompressible flow problems. Here

$$u = \frac{1}{y}\frac{\partial \psi}{\partial y}, v = -\frac{1}{y}\frac{\partial \psi}{\partial x},$$

And vorticity

$$\zeta = \frac{\partial v}{\partial x} - \frac{\partial u}{\partial y} \tag{4}$$

The equations (3) can be written as,

$$\frac{\partial^2 \psi}{\partial x^2} + \frac{\partial^2 \psi}{\partial y^2} + \zeta y = \frac{1}{y}\frac{\partial \psi}{\partial y}, \tag{5}$$

$$\frac{2\alpha^2}{\mathrm{Re}}\frac{\partial \zeta}{\partial t} + \frac{1}{y}\left(\frac{\partial \psi}{\partial y}\frac{\partial \zeta}{\partial x} - \frac{\partial \psi}{\partial x}\frac{\partial \zeta}{\partial y}\right) + \frac{1}{\mathrm{Re}}\left(\frac{\partial^2 \psi}{\partial x^2} + \frac{\partial^2 \psi}{\partial y^2}\right) = -u\zeta - \frac{1}{\mathrm{Re}}\left(u - \frac{\zeta}{y}\right) - M_0(u - v). \tag{6}$$

By taking the partial derivative of equation (1) with respect to y and subtracting the partial derivative of equation (2) with respect to x, the pressure term is eliminated.

The relationships between the physical plane and the transformed plane are given as follows:

$$\frac{1}{J^2}\left(m^{11}\frac{\partial^2 x}{\partial \xi^2} - 2m^{12}\frac{\partial^2 x}{\partial \xi \partial \eta} + m^{22}\frac{\partial^2 x}{\partial \eta^2}\right) - \left(R\frac{\partial x}{\partial \xi} + S\frac{\partial x}{\partial \eta}\right) = 0 \tag{7}$$

$$\frac{1}{J^2}\left(m^{11}\frac{\partial^2 y}{\partial \xi^2} - 2m^{12}\frac{\partial^2 y}{\partial \xi \partial \eta} + m^{22}\frac{\partial^2 y}{\partial \eta^2}\right) - \left(R\frac{\partial y}{\partial \xi} + S\frac{\partial y}{\partial \eta}\right) = 0 \tag{8}$$

The metric coefficient and the Jacobian of the transformation are,

$$m^{11} = \frac{\partial^2 x}{\partial \eta^2} + \frac{\partial^2 y}{\partial \eta^2},\ m^{12} = \frac{\partial^2 x}{\partial \xi^2} + \frac{\partial^2 y}{\partial \xi^2},\ m^{22} = \frac{\partial x}{\partial \xi}\frac{\partial x}{\partial \eta} + \frac{\partial y}{\partial \xi}\frac{\partial y}{\partial \eta},\quad J = \frac{\partial x}{\partial \xi}\frac{\partial y}{\partial \eta} - \frac{\partial x}{\partial \eta}\frac{\partial y}{\partial \xi},$$

The governing equations can be written as a coupled set of equations in terms of the stream function and vortcity. The non-dimensional form in the boundary fitted co-ordinates is,

$$\frac{1}{J^2}\left(m^{11}\frac{\partial^2 \psi}{\partial \xi^2} - 2m^{12}\frac{\partial^2 \psi}{\partial \xi \partial \eta} + m^{22}\frac{\partial^2 \psi}{\partial \eta^2}\right) - \left(R\frac{\partial \psi}{\partial \xi} + S\frac{\partial \psi}{\partial \eta}\right) + y\zeta = S_\psi \tag{9}$$

$$\frac{2\alpha^2}{\mathrm{Re}}\frac{\partial \zeta}{\partial t} + \frac{1}{y}\left(u^{\xi\eta}\frac{\partial \zeta}{\partial \xi} + v^{\xi\eta}\frac{\partial \zeta}{\partial \eta}\right) + \frac{1}{\mathrm{Re}}\left[\frac{1}{J^2}\left(m^{11}\frac{\partial^2 \zeta}{\partial \xi^2} - 2m^{12}\frac{\partial^2 \zeta}{\partial \xi \partial \eta} + m^{22}\frac{\partial^2 \zeta}{\partial \eta^2}\right) - \left(R\frac{\partial \zeta}{\partial \xi} + S\frac{\partial \zeta}{\partial \eta}\right)\right] = S_\zeta - \mathrm{K}_\zeta \tag{10}$$

where

$$u = \frac{1}{Jy}\left(-\frac{\partial x}{\partial \eta}\frac{\partial \psi}{\partial \xi} + \frac{\partial x}{\partial \xi}\frac{\partial \psi}{\partial \eta}\right), \quad v = -\frac{1}{Jy}\left(\frac{\partial y}{\partial \eta}\frac{\partial \psi}{\partial \xi} - \frac{\partial y}{\partial \xi}\frac{\partial \psi}{\partial \eta}\right),$$

$$u^{\xi\eta} = \frac{1}{J}\left(u\frac{\partial y}{\partial \eta} - v\frac{\partial x}{\partial \eta}\right), \; v^{\xi\eta} = \frac{1}{J}\left(v\frac{\partial x}{\partial \eta} - u\frac{\partial y}{\partial \eta}\right), S_\psi = \frac{1}{Jy}\left(-\frac{\partial x}{\partial \eta}\frac{\partial \psi}{\partial \xi} + \frac{\partial x}{\partial \xi}\frac{\partial \psi}{\partial \eta}\right),$$

$$S_\zeta = \frac{1}{Jy}\left[\left(\frac{\partial y}{\partial \eta}\frac{\partial \psi}{\partial \xi} - \frac{\partial y}{\partial \xi}\frac{\partial \psi}{\partial \eta}\right)\zeta - \frac{1}{\mathrm{Re}}\left\{\left(-\frac{\partial x}{\partial \eta}\frac{\partial \zeta}{\partial \xi} + \frac{\partial x}{\partial \xi}\frac{\partial \zeta}{\partial \eta}\right)\right\} - \frac{\zeta}{y}\right],$$

$$\mathrm{K}_\zeta = \frac{\mathrm{K}_0}{Jy}\left(\left(-\frac{\partial x}{\partial \eta}\frac{\partial \psi}{\partial \xi} + \frac{\partial x}{\partial \xi}\frac{\partial \psi}{\partial \eta}\right) + \left(\frac{\partial y}{\partial \eta}\frac{\partial \psi}{\partial \xi} - \frac{\partial y}{\partial \xi}\frac{\partial \psi}{\partial \eta}\right)\right).$$

The parameters Re and α\alphaα vary depending on specific locations within the circulatory system, taking relatively large values in the aorta and major arteries, and significantly smaller values in the arterioles. Their physiological ranges in the human circulatory system are approximately 0–1000 for Re, and 0–15 for α\alphaα, respectively.

2.2 Boundary conditions

Assuming a fully developed Poiseuille flow, it is necessary to specify an upstream inlet location along with the corresponding boundary condition. To achieve this, the velocity profile is defined as follows:

$$\psi = y^2\left(1 - \frac{1}{2y^2}\right), \quad \zeta = -4y, \tag{12}$$

in the transformed plane.

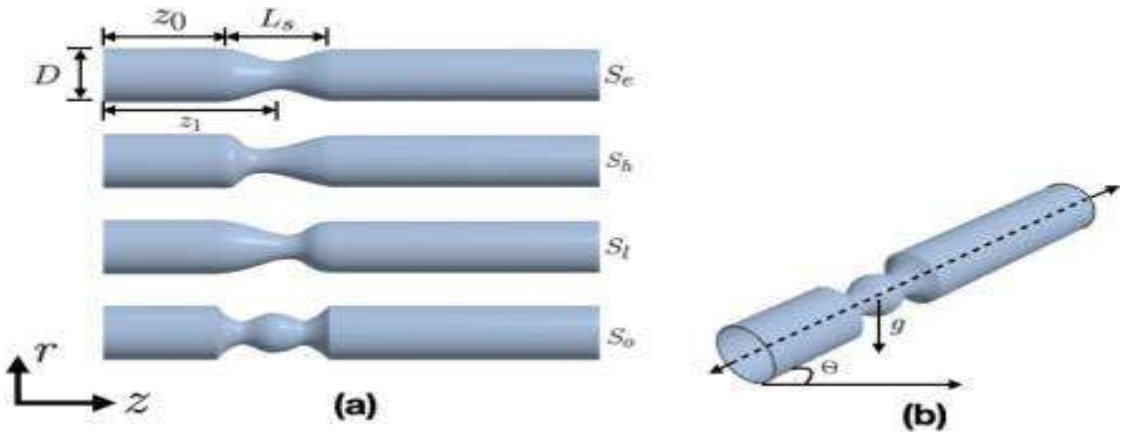

Figure 2. Flow diagram of Stenosis artery

Assuming that the outlet, located downstream, is sufficiently far from the constriction such that the flow field remains unchanged along the axial direction, Neumann boundary conditions are imposed for both the stream function and vorticity.

$$\frac{\partial \psi}{\partial x} = 0, \; \frac{\partial \zeta}{\partial x} = 0 \text{ at } \xi = 1, \text{ and } \quad \psi = 0.5, \; \frac{\partial x}{\partial \eta}\frac{\partial \psi}{\partial \xi} + \frac{\partial x}{\partial \xi}\frac{\partial \psi}{\partial \eta} = 0, \text{ at } \eta = 1 \tag{13}$$

The no-slip requirements are typically the boundary constraints that are applied to the wall.,

i.e. $\frac{\partial \psi}{\partial \tau} = V.n, \quad \frac{\partial \psi}{\partial n} = V.\tau$ (14)

where V is the known velocity on the wall, and τ , n are the unit tangential, normal vectors at the wall .In the present case, the velocity at the wall is zero. The two conditions on ψ are:

$$\psi = 0.5, \quad \frac{\partial x}{\partial \eta}\frac{\partial \psi}{\partial \xi} + \frac{\partial x}{\partial \xi}\frac{\partial \psi}{\partial \eta} = 0, \text{ at } \eta = 1. \tag{15}$$

3. Numerical Method

The spatially discretized form of the governing equations is attained using a standard finite difference scheme. A computational mesh is established in the transformed space, consisting of m×n grid points uniformly distributed in both directions. The superscript denotes the grid point location for the single spatial dimension considered here. The semi-discretized governing equations are expressed as follows:

$$\frac{1}{J^2_{i,j}}\left(\frac{m_{i,j}^{11}}{\Delta\xi^2}D^{\xi}{}_{+}D^{\xi}{}_{-}\psi_{i,j}-\frac{m_{i,j}^{12}}{2\Delta\xi\Delta\eta}D^{\xi}{}_{0}D^{\eta}{}_{0}\psi_{i,j}+\frac{m_{i,j}^{22}}{\Delta\eta^2}D^{\eta}{}_{+}D^{\eta}{}_{-}\psi_{i,j}\right)$$
$$-\left(\frac{R_{i,j}}{2\Delta\xi}D^{\xi}{}_{0}\psi_{i,j}+\frac{S_{i,j}}{2\Delta\eta}D^{\eta}{}_{0}\psi_{i,j}\right)+y_{i,j}\zeta_{i,j}=S_{\psi i,j} \quad (17)$$

$$\frac{2\alpha^2}{\mathrm{Re}}\frac{\partial}{\partial t}\zeta_{i,j}+\frac{1}{y_{i,j}}\left(\frac{u^{\xi\eta}}{2\Delta\xi}D_0{}^{\xi}\zeta_{i,j}+\frac{v^{\xi\eta}}{2\Delta\eta}D_0{}^{\eta}\zeta_{i,j}\right)$$
$$+\frac{2}{\mathrm{Re}}\left[\frac{1}{j^2_{i,j}}\left(\frac{m^{11}{}_{i,j}}{\Delta\xi^2}D^{\xi}{}_{+}D^{\xi}{}_{-}\zeta_{i,j}-\frac{m^{12}{}_{i,j}}{2\Delta\xi\,\Delta\eta}D^{\xi}{}_{0}D_0{}^{\eta}\,\zeta_{i,j}+\frac{m^{22}{}_{i,j}}{\Delta\eta^2}D^{\eta}{}_{+}D_{-}{}^{\eta}\zeta_{i,j}\right)-\left(\frac{R_{i,j}}{2\Delta\xi}D^{\xi}{}_{0}\zeta_{i,j}+\frac{S_{i,j}}{2\Delta\eta}D^{\eta}\zeta_{i,j}\right)\right]$$
$$=S_{\zeta_{i,j}}-K_{\zeta_{i,j}} \quad (18)$$

for i = 2,m-1, j = 2...,n-1.

The difference operators are defined as $D^{\xi}{}_{+}f_{i,j}=f_{i+1,j}-f_{i,j}$, $D^{\xi}{}_{-}f_{i,j}=f_{i,j}-f_{i-1,j}$ and $D^{\xi}{}_{0}f_{i,j}=f_{i+1,j}-f_{i-1,j}$

Similarly, $D^{\eta}{}_{+}f_{i,j}=f_{i,j+1}-f_{i,j}$, $D^{\eta}{}_{-}f_{i,j}=f_{i,j}-f_{i,j-1}$ and $D^{\eta}{}_{0}f_{i,j}=f_{i,j+1}-f_{i,j-1}$,

The discrete form of the above boundary conditions can be imitative using a standard finite difference scheme.

$$\psi_{1,j}=y^2{}_{1,j}\left(1-\tfrac{1}{2}y^2{}_{1,j}\right),\ \zeta_{1,j}=-y_{1,j},\ D^{\eta}{}_{h}y_{m,j}D^{\xi}{}_{h}\psi_{m,j}D^{\eta}{}_{h}\psi_{m,j}=0 \quad (19)$$

$$D^{\eta}{}_{h}y_{m,j}D^{\xi}{}_{h}\zeta_{m,j}-D^{\xi}{}_{h}y_{m,j}D^{\eta}{}_{h}\zeta_{m,j}=0 \quad (20)$$

for j =2 ,..., n-1 ,

$$\psi_{i,1}=0,\ \zeta_{i,1}=0,\psi_{i,n}=0.5,\ D^{\eta}{}_{h}x_{i,n}D^{\xi}{}_{h}\psi_{i,n}+D^{\xi}{}_{h}x_{i,n}D^{\eta}{}_{h}\psi_{i,n}=0 \quad (21)$$

for i =2,...m-1,

where $D^{\xi}{}_{h}f_{i,j}=3f_{i,j}-4f_{i-1,j}+f_{i-2,j}$, $D^{\xi}{}_{h}f_{i,j}=-3f_{i,j}+4f_{i+1,j}-f_{i+2,j}$,

and $D^{\eta}{}_{h}f_{i,j}=3f_{i,j}-4f_{i,j-1}+f_{i,j-2}$, (22)

While all other boundary conditions are conventional, the no-slip condition presents a computational experiment, as the vorticity value at the wall (i.e., at j=nj) is not directly available for solving the difference equations (18). Though discrete boundary conditions involving wall vorticity have been successfully applied, direct implementation of the natural conditions (14) and (15) is acclaimed, as recommended by Huang et al. [1995]. For computational purposes, the following iterative algorithm is employed.

Algorithm:

Step 1: Equation (10) is solved for j=2,...,n−1, and i=2,...,m−1. The stream function (ψ) at j=n−1 is computed using the no-slip boundary conditions (14) at the wall. The resulting algebraic equations are solved using the Gauss–Seidel method.

Step 2: Update $u^{\xi\eta}$ and $v^{\xi\eta}$ using ψ from the previous step.

Step 3: To calculate ζ at j = n-1 for i = 1,..., m-1 to relation equation (10), coupling ψ and ζ, is fulfilled at j = n-1.
Step 4: Solve equation (11) at j = 2, ...,n-1 for i = 2, ...,m-1using the value at j = n-1 from step (3) and essential conditions at the other boundaries. Again the algebraic equations are explained by using Gauss-Siedal method .The time dependent term is dropped out and under relaxation is applied when compulsory.
Step 5: Steps (1)-(4) are repetitive until convergence is extended.

For temporal discretization, a Crank-Nicolson-type approach is used to guarantee second-order accuracy for the convection and diffusion terms in both time and space. The identical iterative process as in the steady-state illustration is used to solve the system at each time step.

5. RESULTS AND DISCUSSION

The proposed model is simple to implement and provides valuable insights into the dependence of shear stress on stenosis geometry, porous effects, and flow conditions—serving as a useful tool for biomedical researchers. Our predictions for wall shear stress show good agreement with the limited experimental data available. The primary objective of this numerical investigation is to develop a comprehensive understanding of how the flow field is influenced by the Reynolds number and the geometry of the stenosis—specifically its height H and length L, measured in units of the arterial radius.
Previous numerical studies by Huang et al. (1995) and Back and Crawford (1992) reported shear stress distributions in stenosed geometries. The five stenoses modelled by Huang et al. (1995) are smooth and conical in shape. In this study, the stenosis models are categorized into three groups: mild (M_1), moderate (M_2), and severe (M_3, M_4, and M_5). The area reduction due to the stenosis is categorized by R(2−R).The axial locations of flow separation and reattachment points, beginning from the point of minimum constriction, are of significant physiological relevance. Meanwhile the simulations are carried out under laminar flow assumptions, discrepancies between our results and those from other studies become more pronounced at higher Reynolds numbers.

Table 1: Geometric parameters of the stenosis models.

	M_1	M_2	M_3	M_4	M_5
H	1/5	1/4	1/3	1/3	1/3
L	5	5	5	10	3
Area reduction (%)	46	57	80	80	80

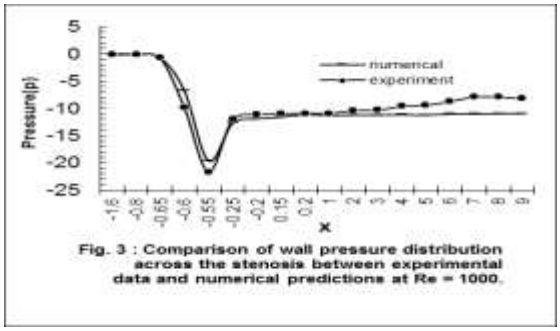

Fig. 3 : Comparison of wall pressure distribution across the stenosis between experimental data and numerical predictions at Re = 1000.

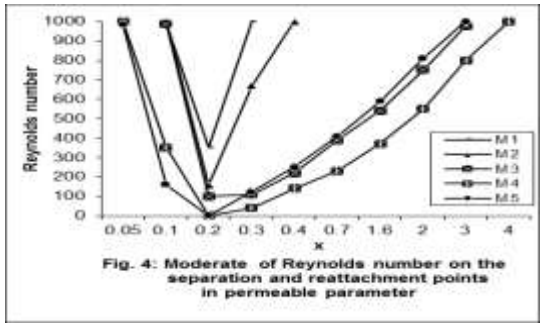

Fig. 4: Moderate of Reynolds number on the separation and reattachment points in permeable parameter

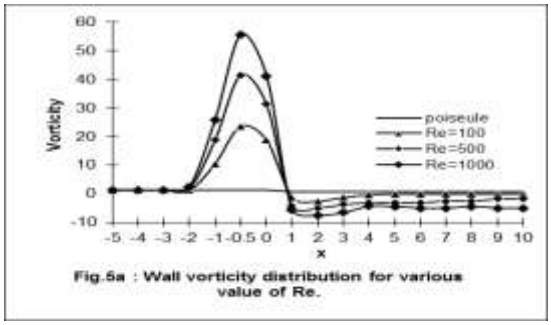

Fig.5a : Wall vorticity distribution for various value of Re.

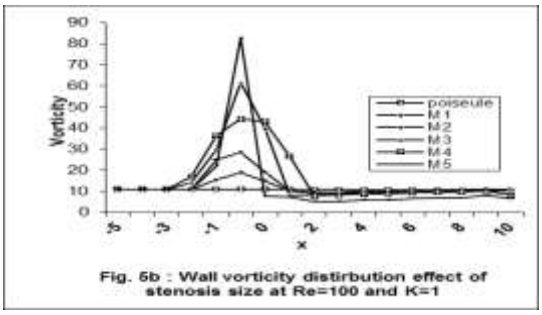

Fig. 5b : Wall vorticity distirbution effect of stenosis size at Re=100 and K=1

Our model successfully captures this feature and demonstrates its applicability across the physiological range of arterial Reynolds numbers. Figure 3 presents the pressure distribution at various Reynolds numbers, while Figure 4 illustrates the influence of both Reynolds number and stenosis size on key flow parameters.

It is evident that the separation length increases almost linearly with the Reynolds number for all stenosis models. The locations of flow separation and reattachment are highly sensitive to both the height and length of the stenosis, particularly under the influence of a magnetic field. At higher Reynolds numbers, flow separation occurs earlier in the case of severe stenosis (M_3, M_4, and M_5), although the separation and reattachment locations differ slightly among these models despite having the same area reduction. In contrast, separation occurs later for the moderate stenosis (M_1 and M_2).

The present numerical method slightly underestimates shear stress values but accurately captures the overall trend observed in available data. Although the three severe stenosis exhibit the same contraction, our results confirm a systematic increase in wall shear stress with decreasing stenosis length in the permeability parameter.

Figure 5 a shows the vorticity distribution along the solid wall for the moderate stenosis (M_2) at various Reynolds numbers. The peak vorticity is observed just upstream of the minimum constriction plane, and this peak shifts slightly upstream with increasing Reynolds number. Downstream of the constriction, the vorticity decays rapidly, following a trend similar to that observed in classical Hagen–Poiseuille flow.

Re	M_1	M_2	M_3	M_4	M_5	Poiseuille
100	9.3	14.2	37.7	29.7	48.9	2.2
500	77.1	120.6	322.9	245.4	423.6	11.7
1000	167.3	278.2	789.2	609.8	1028.8	22.3

Table 2: Calculated peak shear stress (in dyn/cm²) for stenosis models M1–M5 across a Reynolds number range of 100 to 1000.

Figure 5b displays the wall vorticity distribution for all stenosis models at a Reynolds number of 100. A significant region of recirculation is observed in the case of severe stenoses (M_3, M_4, and M_5), as indicated by the presence of negative vorticity values.This study examines steady flow within a physiologically relevant Reynolds number range, incorporating the effects of wall porosity for all stenosis models. Table 2 presents the maximum wall shear stress values for the five models, along with reference values corresponding to fully developed Poiseuille flow. The results show that wall shear stress—peaking just upstream of the minimum constriction—is significantly amplified as the lumen area decreases. Experimental studies on animals have shown that blood flow is not noticeably diminished even when the degree of stenosis exceeds 75%. Thus, the shear stress values associated with 75% area reduction (models M_3, M_4, and M_5) can be considered conservative estimates.
The application of the permeability parameter as a flow control mechanism is particularly relevant in cases involving cholesterol-related arterial blockage, offering potential therapeutic implications.

6. CONCLUSION

Using computational methods, a simplified model of blood flow in a stenosed artery has been studied; the findings are in good agreement with experimental evidence that is accessible in the literature. The quantitative results indicate that vascular disease is unlikely to develop as a result of excessive shear stress alone.Numerical forecasts and experimental data showed a significant correlation, especially in areas close to the stenosis. In the context of specific medical problems, the present study illustrates the possibility of permeable flow control in the treatment of stenosed arteries.t is evident from the numerical results that mean flow parameters alone cannot be used to draw conclusions about fluid dynamic effects in atherosclerosis. The fundamental mechanism driving this correlation is still unknown, though, and more research is necessary to draw firm conclusions. When assessing the possible health benefits to individuals as well as the expenditures of healthcare, these models might offer insightful information. Health districts with diverse populations, such as those with sizable ethnic minority populations who are more likely to develop diabetes, will find this very helpful. Plaques restrict blood flow by causing connective tissue to grow inward and deposit cholesterol on the arterial wall. Understanding the part hemodynamic factors play in the pathophysiology and course of sickness would also be very helpful. Through numerical simulation, it is possible to get detailed flow patterns associated with analytical stenosis without intrusive procedures. The models provide details on how to evaluate the costs and advantages to an individual's health. A more thorough investigation of such a complicated issue will require more sophisticated and physiologically accurate models. The current results, however, are useful since they offer in-depth understanding of the flow field, which can be the basis for further investigation.

REFERENCES

1. Banerjee, R. K., Cho, Y. I. and Back, L. H. (1993): Numerical studies of three-dimensional arterial flows in reverse curvature geometry. Part I- Peak flow. Trans. ASME J. Biomech.Engg. 115, 316-326.
2. Bharadvaj, B.K., Mabon, R.F., and Giddens, D.P. (1982 a, b): Steady flow in a model of the human carotid bifurcation. Part I-Flow visualisation. Part II-Laser Doppler anemometer measurements. J. Of Biomechanics' 15, 349-362.
3. Boesiger. P., Maier, S. E., Kecheng, L., Scheidegger, M. B., Meier, D. (1982): Visualisation and quantification of the human blood flow by magnetic resonance imaging. J. Of Biomachanics 25. 55-67.
4. Botnar, R., Scheidegger, M. B., Boesiger, P. (1996): Quantification of blood flow patterns in human vessels by magnetic resonance imaging. Technology and Health Care 4, 97-112.
5. Botnar, R., Rappitch, G., Scheidegger, M. B., Liepsch, D., Perktold, Boesiger, P. (2000): Hemodynamics in the carotid artery bifurcation: a comparison between numerical simulation and in vitro MRI measurements. J. Bio mechanics 33,137-144.
6. Huang, H., Modi, V. J., and Seymour (1995): Fluid mechanics of stenosed arteries. Int. J. of Engg. Sciences. 33, 6, 815-828.
7. Ku, D. N. (1997): Blood flow in arteries. Annual Review of Fluid Mechanics, 29,399-434.
8. Perktold, K. and Rappitsch, G. (1995): Computer simulation of local blood flow and vessel mechanics in a compliant carotid artery bifurcation model. J. Bio mechanics' 28,845-956.

9. Rachev, A., Stergiopelos, N., Meister, J.J. (1998): A model for geometric and mechanical adaptation of arteries to sustained hypertension. J. Of Biomechanical engg.
120, 9-17
10. Rees, J. M. and Thompson, D. S. (1999) : Shear stress in arterial stenoses: a momentum integral model. J. Biomechanics. 31, 1051-1057.
11. Reuderink, P. J. (1991): Analysis of the flow in a 3D distensible model of the carotid artery bifurcation. Ph.D. thesis, University of Eindhoven, The Netherlands.
12. Rieu, R., Pelissier, R., and Farahifar, D. (1989): An experimental investigation of flow characteristics in bifurcation models. Eur. J. Mech. 8(1), 73-101.
13. Rindt, C. C. M., Van de Vosse, F. N., Van Steenhoven, A. A., Janssen, J. D., and Reneman, R. S. (1987): A numerical and experimental analysis of the human carotid bifurcation. J. Of Biomechanics 20, 499-509.
14. Sharma, G.C. and Kapur, J. (1995): Finite element computations of two-dimensional arterial flow in the presence of a transverse magnetic field. International J. for numerical methods in fluid dynamics. Vol. 20 pp. 1153-1161.
15. Zendehbudi, G.R. and Moayari, M. S. (1999) : Comparison of physiological and simple pulsatile flows through stenosed arteries. Journal of Biomechanics vol.32, pp. 959-965.
16. Anil Kumar, G.C. Sharma and Madhu Jain(2001): Finite element Galerkins approach for a computational study of arterial flow, Applied Mathematics and Mechanics 22(9), pp 1012-1018, 2001
17. Anil Kumar Gupta (2011): Performance Model and Analysis of Blood Flow in Small Vessels with Magnetic Effects, International Journal of Engineering, IJE Transactions A: Basics, Vol. 25, No. 2, pp 190 -196, , ISSN 1728-1431(print)/ 1735-9244 (e- print) published December 15, 2011 Iran
18. Anil Kumar Gupta (2011)**:** Performance and analysis of blood flow through carotid artery, International Journal of Engineering and Business Management Vol. 3, No. 4, pp 1-6,
19. Anil Kumar Gupta (2009): Finite Element Galerkin's scheme for flow in blood vessels with magnetic effects, International Journal of Applied Systemic Studies, vol. 2 (3) pp- 284-293, Indersciecnce publishing, ISSN 1751-0589 (Print)/ 1751-0597 (Online) UK.
20. R. K. Saket and Anil Kumar(2008): Reliability of convective diffusion process in porous blood vessels, Chemical Product and Process Modeling, Vol.(3) Article (25) ISSN: 1934-2659, Canada 2008.
21. Anil Kumar, CL Varshney and GC Sharma (2005): Computational technique for flow in blood vessels with porous effects, Applied Mathematics and Mechanics 26(1) pp 63-72, 2005.
22. Anil Kumar, C L Varshney and GC Sharma (2005): Performance modeling and analysis of blood flow in elastic arteries, Applied Mathematics and Mechanics, **26**(3) ,pp 345–354.
23. T. Salahuddin, M. Nazir, M. Khan, Shah M., Muhammad I. (2025), Blood flow study in stenotic arteries through porous medium with heat generation, International Communications in Heat and Mass Transfer, Volume 164, Part B, 108894.
24. Lubna Sarwar, Azad Hussain, Flow characteristics of Au-blood nanofluid in stenotic artery, International Communications in Heat and Mass Transfer, Volume 127, 2021, 105486.